THE ASTROPHYSICAL JOURNAL, 462:32–49, 1996 May 1

GALAXY CLUSTER VIRIAL MASSES AND Ω

R. G. CARLBERG,[1,2] H. K. C. YEE,[1,2] E. ELLINGSON,[1,3] R. ABRAHAM,[1,4,5] P. GRAVEL,[1,2]
S. MORRIS,[1,5] AND C. J. PRITCHET[1,6]

Received 1995 September 6; accepted 1995 October 6

ABSTRACT

The mean density of the universe is equal to the mass of a large galaxy cluster divided by the equivalent comoving volume in the field from which that mass originated. To reexamine the rich cluster Ω-value the CNOC Cluster Survey has observed 16 high X-ray luminosity clusters in the redshift range 0.17–0.55, obtaining approximately 2600 velocities in their fields. The systemic redshift, the rms line-of-sight velocity dispersion σ_1, and the mean harmonic radius r_v are derived for each cluster using algorithms that correct for interlopers in redshift space and measure the angular extent of the sampling. The virial mass, and its internal error, are derived from σ_1 and r_v. The cluster luminosity is estimated from the K-corrected r-band luminosities of the cluster galaxies. Directly adding all the light to $M_r^K = -18.5$ mag, about $0.2L_*$, and extrapolating for the small amount of light below the limit, the average mass-to-light ratio of the clusters is $295 \pm 53\ h\ M_\odot\ L_\odot^{-1}$, and the average mass per galaxy to $M_r^K = -19.0$ mag is $4.2 \pm 1.1 \times 10^{12}\ h^{-1}\ M_\odot$. The clusters are consistent with having a universal M_v/L-value (within the errors of about 25%) independent of their velocity dispersion, mean color of their galaxies, blue galaxy content, redshift, or mean interior density. Using field galaxies within the same data set, with the same corrections, we find that the closure mass-to-light ratio, ρ_c/j, is $1025 \pm 140\ h\ M_\odot\ L_\odot^{-1}$, and the closure mass per galaxy to $M_r^K = -19.0$ mag, ρ_c/Φ, is $15.5 \pm 3.0 \times 10^{12}\ h^{-1}\ M_\odot$. Under the assumptions that the galaxies are distributed like the mass and that the galaxy luminosities and numbers are statistically conserved, assumptions that these data indirectly support, $\Omega_0 = 0.24 \pm 0.05 \pm 0.09$, where the errors are, respectively, the 1 σ random error and an estimate of the possible systematic error resulting from the normalization to galaxy content.

Subject headings: cosmology: observations — galaxies: clusters: general — galaxies: fundamental parameters

1. INTRODUCTION

Clusters of galaxies are the largest collapsed objects in the universe and play a particularly important role in the problem of estimating the mean density of matter that participates in gravitational clustering, ρ_0. The standard procedure is as follows. The mass of a cluster, within some radius, is measured with any of a number of techniques, such as galaxy kinematics, X-ray profiles, or gravitational lensing. To relate cluster masses to $\rho_0 = M/V$ requires an estimate of the comoving volume, V, from which the clusters collapsed, normally done via the luminosity of the cluster galaxies, L, in ratio to the field luminosity density, j, so that $V = L/j$. The value of $\Omega_0 \equiv \rho_0/\rho_c$ can therefore be rewritten as the cluster mass-to-light ratio, M/L, divided by the closure mass-to-light ratio, $(M/L)_c \equiv \rho_c/j$. The quantity Ω_0 is independent of H_0 and determines the future of the expansion of the universe, in the absence of a cosmological constant or a "hot" component of the mass field. The classical cluster mass estimator is the virial mass, M_v, a straightforward global estimator suitable for relatively sparse data (but see Bahcall & Tremaine 1981). This subject has a long history with relatively stable results. That is, the virial mass-to-light ratios of clusters, M_v/L, are generally in the range $200–400\ h\ M_\odot\ L_\odot^{-1}$ (see, e.g., Zwicky 1933, 1937; Smith 1936; Schwarzschild 1954; Gunn 1978; Ramella, Geller, & Huchra 1989; David, Jones, & Forman 1995; Bahcall, Lubin, & Dorman 1995), which, in ratio to $(M/L)_c \simeq 1500\ h$ (Efstathiou, Ellis, & Peterson 1988; Loveday et al. 1993), indicates $\Omega_0 \simeq 0.2$.

The low value of Ω_0 from cluster M_v/L measurements is not accepted as a definitive measurement of the field value of Ω_0, mainly because there are uncontrolled systematic errors in both the mass and the light measurements that potentially allow the cluster M_v/L ratios to be consistent with $\Omega = 1$. That is, the reliability of the virial mass statistic as indicating the total gravitational mass of a cluster is critically dependent on whether the galaxy distribution traces the total mass distribution of the cluster. The possibility that the total mass distributions of galaxy clusters are more extended than their constituent galaxies has been recognized for many years (Limber 1959; West & Richstone 1988; Carlberg 1994). The virial mass is a usefully accurate measurement of the mass within the orbits of the galaxies and completely independent of any anisotropy of the velocity ellipsoid, but if the cluster light is more concentrated than the cluster mass, then the virial mass will be an underestimate of the total mass. This assumption that the mass and galaxies are similarly distributed is straightforward to test given sufficient data to derive radially resolved luminosity and velocity dispersion profiles. The large color differences between cluster and field galaxies implies that their recent star formation histories are different, which may simply be a recent decline associated with infall into the

[1] Visiting Astronomer, Canada-France-Hawaii Telescope, which is operated by the National Research Council of Canada, le Centre National de Recherche Scientifique, and the University of Hawaii.
[2] Department of Astronomy, University of Toronto, Toronto ON, M5S 1A7 Canada.
[3] Center for Astrophysics and Space Astronomy, University of Colorado, CO 80309.
[4] Institute of Astronomy, Madingley Road, Cambridge CB3 OHA, UK.
[5] Dominion Astrophysical Observatory, Herzberg Institute of Astrophysics, National Research Council of Canada, 5071 West Saanich Road, Victoria, BC, V8X 4M6, Canada.
[6] Department of Physics and Astronomy, University of Victoria, Victoria, BC, V8W 3P6, Canada.

cluster, or, it may indicate drastically different star formation efficiencies at early times (Dressler 1980; Dressler & Gunn 1983; Butcher & Oemler 1984; Yee et al. 1995c) with the consequence that the luminosity per unit mass could be quite different between cluster and field. All of these assumptions are testable given an appropriate data set.

Dynamical mass measurements have the benefit that their strengths and weaknesses are already relatively well understood and are easily studied further with n-body simulations. Although not of direct interest here, dynamical mass estimation can be extended to well beyond the virialized region by measuring peculiar velocities in the infall region, in which case the results depend on the biasing of galaxies with respect to the mass field. In this paper we determine dynamical masses for a sample of 16 clusters at moderate redshift. Spectroscopic and photometric data were obtained for these clusters as part of the CNOC (Canadian Network for Observational Cosmology) cluster redshift survey (see, e.g., Carlberg et al. 1994; Yee, Ellingson, & Carlberg 1996b). The overall goal of this project is to measure the total mass and luminosity contained within the central virialized region of the cluster to establish a value of Ω and measure any biases among cluster galaxies, cluster mass, and field galaxies. Beyond the virialized region there is an infalling mixture of galaxies, gas, and dark matter, which is very likely statistically identical to the field. Other than the few very red central galaxies and the cD, the bulk of the cluster galaxy population is likely to be composed of infallen field galaxies. Because our sample of galaxies extends from the cluster core to the distant field we can check whether galaxy population modifications occur only in the virialized region of the cluster. Therefore, any systematic changes in the mass-to-light ratio resulting from either galaxy differences or a true mass-to-light segregation will be measurable, increasing the accuracy of our Ω result.

The twin complications for interpreting redshifts are that cluster galaxies and surrounding highly correlated field galaxies are intermingled in redshift space, and, individually clusters are quite nonspherical and internally clumpy, with the velocities at large radii being influenced by surrounding large-scale structure. Hence, there are two main requirements for a successful measurement: accurate control of the background and a sufficiently large sample to average over the aspherical complications of single clusters. A feasibility study (Carlberg et al. 1994) showed that approximately 1000 galaxy velocities and a comparable number of field velocities distributed over 10 or so cluster fields is sufficient to indicate whether the virial mass is the total mass of the clusters. The built-in field sample allows a study of the relative galaxy populations of cluster and field, and the closure mass-to-light ratio and mass per galaxy.

There is no question that the cluster M_v/L technique gives, in principle, an accurate Ω-value. The key issues are to constrain the technique's systematic errors and minimize its random errors. The main areas of concern are the accuracy of the virial mass and galaxy population differences between the cluster and the field. Our data allow these problems to be addressed using our sample alone, since it contains more than 1000 field galaxies, and offers the considerable benefit of homogeneous selection as discussed in § 2. In § 3 the cluster rms velocity dispersions and mean harmonic radii are derived. These quantities are used to find virial masses in § 4. The luminosity and numbers of cluster galaxies are used in § 5 to give M_v/L and M_v/N ratios. The field values of these quantities are derived in § 6, and the resulting Ω-values are derived in § 7. Companion papers examine the relative light and mass profiles of the clusters (Carlberg, Yee, & Ellingson 1996a) and Ω from blue and red subsamples (Carlberg et al. 1996b).

2. SAMPLE AND OBSERVATIONS

Clusters at moderate redshifts, $z \simeq \frac{1}{3}$, have a number of advantages for mass estimation. They are sufficiently distant that they have a significant redshift interval over which the density of foreground and background galaxies are nearly uniformly sampled in redshift. An accurate background estimate is crucial for measurements in the outskirts of the cluster profile. Clusters at higher redshifts have relatively more blue galaxies (Butcher & Oemler 1984) than those at low redshift, which increases the similarity between cluster galaxies and field galaxies (but they are by no means identical). Since the mean galaxy color varies within our sample, the effect of varying galaxy types on the total luminosity can be measured.

There are a number of practical considerations that motivate our choice of clusters. At $z \simeq \frac{1}{3}$, a comoving Abell diameter of $3\,h^{-1}$ Mpc spans an angle of about 12′, which is sufficiently small that uniformity of photometry and sample selection is relatively easily assured. This size is also comparable to the field size of the Canada-France-Hawaii Telescope (CFHT) Multiple-Object-Spectrograph (MOS), approximately 10′ square (LeFèvre et al. 1994). These clusters are also ideal targets for other types of mass measurement observations, such as gravitational lensing and X-ray plasma profiles.

Our cluster sample was selected from the *Einstein* Medium Sensitivity Survey Catalog (Gioia et al. 1990; Henry et al. 1992; Gioia & Luppino 1994), which is a collection of serendipitous objects discovered in X-ray images taken for other purposes. For our survey we chose clusters with $z \geq 0.18$ (a consequence of the poor blue response of the CCDs then available) and in the declination range, $-15 \leq \delta \leq 65$, most suitable for CFHT. To select uniformly clusters that are likely to be rich in galaxies, have a large velocity dispersion (both of which make the measurement relatively easier), and are guaranteed to have a substantial virialized component, we chose those with $L_x \geq 4 \times 10^{44}$ ergs s^{-1} and $f_x \geq 4 \times 10^{-13}$ erg cm^{-2} s^{-1}. Two clusters were added to fill R.A. gaps: MS 1231+15 has an X-ray luminosity below our limit, and Abell 2390, a rich cluster (Abell 1958), is a high X-ray luminosity (Ulmer et al. 1986) cluster from another catalog. On the whole, the large X-ray luminosities of these clusters indicate that they are at least partially virialized.

Observations were made at CFHT in 24 assigned nights in 1993 January, June, and October and 1994 January and March. The observational techniques and data reduction are described in Yee, Ellingson, & Carlberg (1996b, hereafter YEC), and the data will be described in a series of papers (see, e.g., Yee et al. 1996a). The fields (either E-W or N-S strips between 9′ and 45′ wide and about 8′ high across the cluster center) were imaged with the Multi-Object Spectrograph (LeFèvre et al. 1994) from which Gunn g- and r-magnitudes are derived, and masks of spectrograph entrance slits were designed for the nonstellar images. The wavelength range of the spectra was shortened with band-limiting filters chosen to match the cluster's redshift, which typically allowed about 100 targets to be observed on a

1996ApJ...462...32C

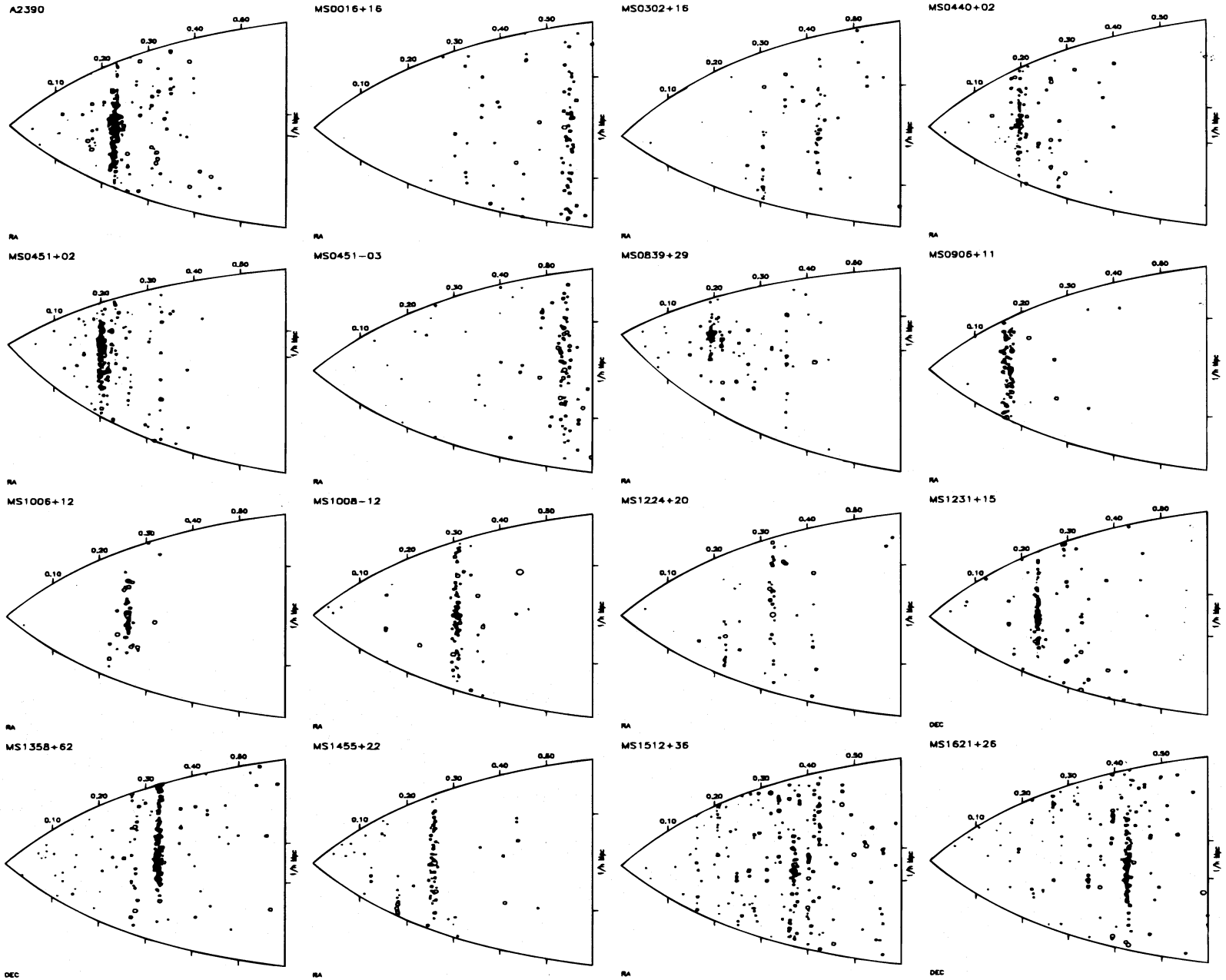

FIG. 1*a*

FIG. 1.—Redshift vs. longest sky axis measured from the brightest cluster galaxy direction for the full fields of the 16 clusters. The redshift increases from the vertex of the diagram, and sky angle is converted to a transverse distance in physical coordinates. Panel (*a*) shows the entire redshift range, panel (*b*) expands the region near the cluster, marking the cluster redshift range with dashed lines.

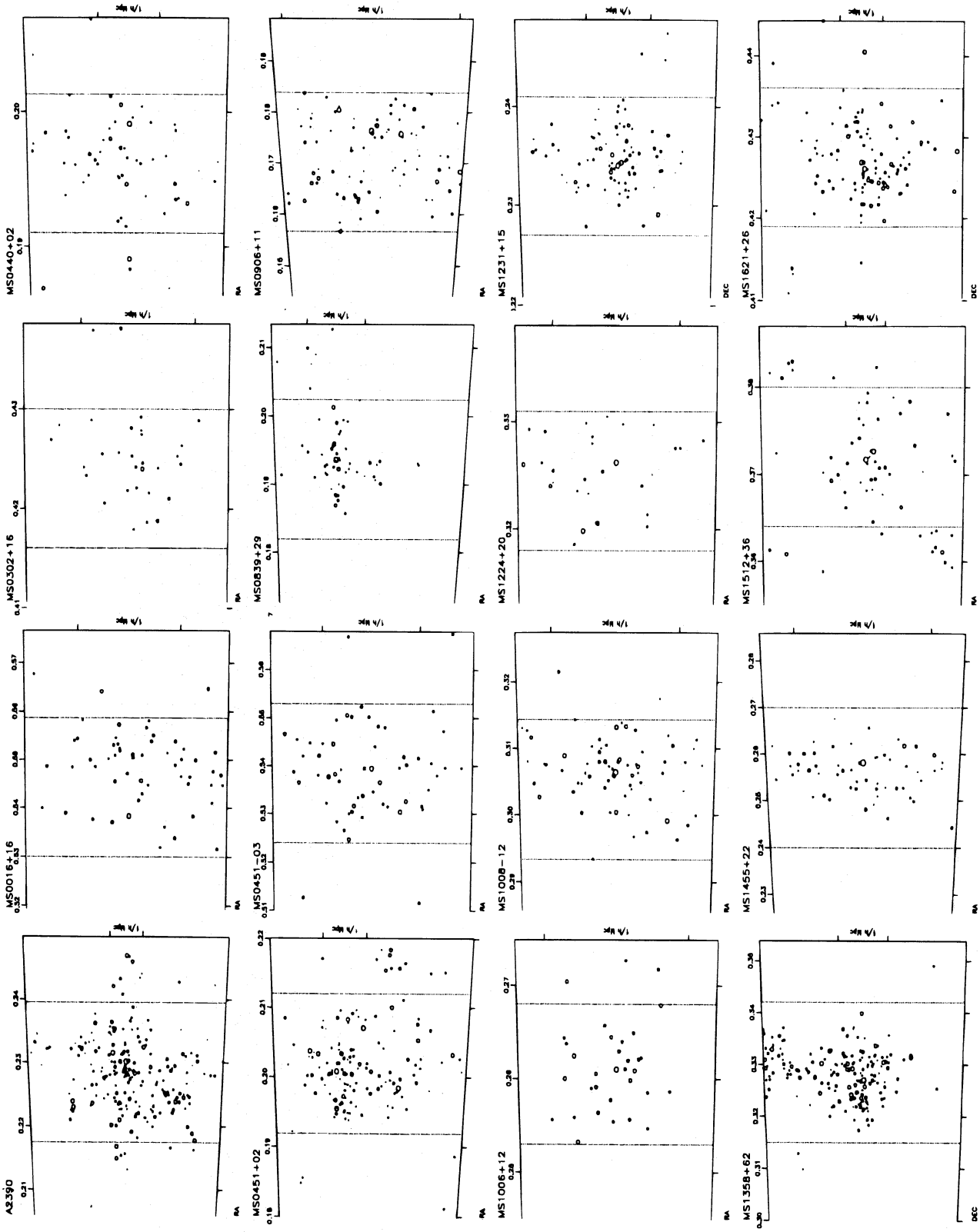

FIG. 1*b*

single mask. The limiting magnitude for spectroscopy for each cluster is set to optimize the number of cluster (as opposed to field) redshifts obtained. The resulting spectra are cross-correlated with a set of templates to give velocities accurate to about 100 km s^{-1} in the rest frame of the cluster. The resulting "pie diagrams" for the entire sample are shown in Figure 1*a* and in the cluster vicinity in Figure 1*b*. Redshift increases with distance from the vertex of the pie diagram, and the angular coordinate is the physical separation in the R.A. or decl. direction, whichever is larger, with the zero coordinate being at the location of the brightest cluster galaxy (which is not necessarily at the center of the observed field).

The fraction of galaxies for which we assign slits and obtain redshifts decreases for fainter galaxies. Such a selection function, which decreases with magnitude, optimizes the rate of return of cluster redshifts but needs to be carefully measured to reconstruct statistically the properties of the complete sample. The algorithm for deciding which galaxies will be assigned spectroscopic slits has the highest priority at the expected m_* of the cluster. The resulting $n(m)$ of the subsample with redshifts is nearly constant with magnitude, whereas the total numbers rise with magnitude. The redshift sample is assigned magnitude selection weights, $w_m(m_r)$, such that their sum gives the total number of objects (or total flux) in the full photometric catalog. The limiting magnitude is defined here as m_r, where $w_m = 5$. The MOS has approximately a fixed number of slits per unit sky area (about 100 in 100 square arcmin), hence there is also a geometric selection weight, $w_g(m_r, x, y)$. The defining relations for these weights are described in YEC. All the results given below incorporate these weights as is appropriate.

In this paper, all distance-dependent quantities are calculated assuming a Hubble constant of 100 km s^{-1} Mpc^{-1}, a deceleration parameter $q_0 = 0.1$, and a cosmological constant $\Lambda = 0$. The choice of q_0 is for approximate consistency with the most straightforward interpretation of our results. The dependence of distance and luminosity on q_0 largely cancels for the evaluation of Ω because it is defined relative to the field in the same redshift range. Our luminosities are K-corrected, but no evolution correction is applied, because as a differential measurement any correction applied equally to the field and the cluster makes essentially no difference to the result. These corrected quantities should only be compared to others that are adjusted to our photometric system. Hence, care should be exercised in any direct comparison of our corrected $z \sim \frac{1}{3}$ quantities to similar quantities at $z = 0$. This caution is particularly important for the mass-to-light ratios.

3. CLUSTER DYNAMICAL PARAMETERS

The redshifts and positions of galaxies are used to define a characteristic velocity and a characteristic length scale of the cluster. As a consequence of the virial theorem, the rms velocity dispersion has the important property that in a spherical system its value is completely independent of any variation in the shape of the velocity ellipsoid. For a triaxial object the line-of-sight rms velocity does depend on viewing angle, which is precisely why we want to average over a dozen or so clusters. The line-of-sight velocity dispersion of a cluster is defined as

$$\sigma_1^2 = \left(\sum_i w_i\right)^{-1} \sum_i w_i (\Delta v_i)^2 , \qquad (1)$$

where the $\Delta v_i = c(z_i - \bar{z})/(1 + \bar{z})$ are the peculiar velocities in the frame of the cluster and $\bar{z}$ is the weighted mean redshift of the cluster. The weights used in equation (1) are magnitude-dependent geometric weights. Unweighted velocities give similar results.

The virial mass estimator normally uses the projected mean harmonic pointwise separation

$$R_H^{-1} = \left(\sum_i w_i\right)^{-2} \sum_{i<j} \frac{w_i w_j}{|\boldsymbol{r}_i - \boldsymbol{r}_j|} , \qquad (2)$$

where the ij sum is over all pairs. Being a pairwise quantity, R_H is sensitive to close pairs and is quite noisy (Bahcall & Tremaine 1981). Furthermore, there is no straightforward way to correct R_H for the approximately rectangular "window" which encloses our cluster sample. That is, simply weighting with the fraction of a circular aperture that is enclosed within our rectangle leads to a systematic underestimate of R_H.

Here we introduce an alternate estimate of R_H. A pair of galaxies at projected coordinates $\boldsymbol{r}_i$ and $\boldsymbol{r}_j$ are statistical representatives of all galaxies at those projected radii. Under the assumption of axial symmetry the angle between these two vectors is a uniform random variable. Hence, some immediate averaging is possible by imagining that one (or the other) of the particles has its mass distributed like a ring, with a radius equal to its radial location with respect to some cluster center. More formally, the expectation value for random angles of the pairwise potential $1/|\boldsymbol{r}_i - \boldsymbol{r}_j|$ is the potential between a point and a ring, which is (noting that the result is independent of the sign of the cosine function for an integral over a circle)

$$R_h^{-1} = \left(\sum_i w_i\right)^{-2} \sum_{i<j} w_i w_j \frac{1}{2\pi} \int_0^{2\pi} \frac{d\theta}{\sqrt{r_i^2 + r_j^2 + 2 r_i r_j \cos\theta}}$$
$$= \left(\sum_i w_i\right)^{-2} \sum_{i<j} w_i w_j \frac{2}{\pi(r_i + r_j)} K(k_{ij}) , \qquad (3)$$

where $k_{ij}^2 = 4 r_i r_j/(r_i + r_j)^2$ and $K(k)$ is the complete elliptic integral of the first kind in Legendre's notation (Press et al. 1992). The quantity R_h will be referred to as the ringwise projected harmonic mean radius. Unlike the original R_H this modified R_h requires an explicit choice of the cluster center and assumes that the cluster is symmetric about the center. Neither of these pose any practical difficulties.

Galaxy clusters are significantly flattened (see, e.g., Plionis, Barrow, & Frenk 1991). The R_h estimator will always overestimate the true R_H for a flattened distribution and a substantially subclustered distribution. The overestimate is compounded if the field sampled happens to lie along the major axis of the cluster. To estimate the size of this effect we calculate the R_h/R_H ratio within completely sampled circles, finding it to be 1.28 ± 0.05 (excluding MS 0906+11, see below). There is no evidence within this sample that the R_h/R_H ratio in a circle correlates with the M/L ratio of the clusters, so we approximate the bias as being uniform. Accordingly, all the R_h are uniformly reduced by this factor.

There are two substantial benefits to be had from the definition of R_h in equation (3). For close pairs the divergence is logarithmic instead of $1/r$, which makes R_h less noisy than R_H. Of immediate practical interest here is that the value of R_h is readily determined for data sets where a strip (sometimes of varying width) across the center has been sampled. For instance, any of our strips can be artifi-

cially narrowed to test how much R_h varies. For a factor of 2 reduction in the width of the A2390 data, R_H declines from 669″ (already a substantial underestimate) to 484″, whereas R_h drops from 831″ to 803″.

The three-dimensional virial radius, r_v, is $r_v = \pi R_h/2$ (Limber & Mathews 1960). With σ_1 and r_v the virial mass of a cluster is calculated as

$$M_v = \frac{3}{G}\sigma_1^2 r_v . \quad (4)$$

3.1. *Cluster Membership and Velocity Dispersions*

The complication in applying equations (1) and (3) to redshift data is to decide which galaxies belong to the cluster and which are likely to be interlopers in redshift space. Because galaxy groups and other clusters have such a high clustering probability near a rich cluster this background is not expected to be smooth. Our magnitude distribution of galaxies with redshifts was designed to maximize the abundance of cluster galaxies and minimize the background. That is, the number of field galaxies per magnitude, $n(m)$, rises steeply with magnitude, $n(m) \propto 0.4m$, whereas the cluster luminosity function is much shallower, $n(m) \propto 0.25m$ or less, below m_*, the characteristic brightness of a cluster galaxy. For each cluster we estimated m_* and then set our spectroscopic exposures so that we expected to obtain redshifts down to the magnitude where cluster galaxies are starting to become less numerous than field galaxies, which in our redshift range and for these rich clusters typically occurs 2 to 3 mag below m_*. The priority list is based on the absolute difference between the galaxy brightness and the cluster m_*. Besides being an efficient procedure, this strategy also ensures that the cluster has the maximum possible contrast in redshift space from the field, as shown in Figure 1. A sampling that is more complete or deeper would mainly provide more field galaxies. The present sample is a reasonably optimal tradeoff between having enough clusters to average out cluster details and having enough galaxies per cluster to obtain satisfactorily accurate measurements of the global properties of each cluster. If more data were obtained, the best strategy would be to first increase the area sampled at large radius in each of the current clusters.

The calculation of the rms velocity dispersion of a cluster uses only the redshifts with no positional information. Defining the extent of rich clusters in redshift space is a relatively difficult problem in general (see, e.g., Bird & Beers 1993; Bird 1995) because cluster members moving at a large velocity with respect to the center of the cluster are impossible to distinguish from field galaxies. Furthermore, many statistical tests to assess the membership status of galaxies in the tails of the velocity distribution are based on the assumption that the underlying distribution is a unimodal Gaussian, which is generally not true for such a kinematically complex system as an accreting cluster and the surrounding large-scale structure. We have reduced the problem through the magnitude distribution of our cluster sample, which provides data that leave clusters as cleanly defined as possible in redshift space.

The procedure for defining the redshift range of the cluster is a manually iterated procedure, roughly equivalent to measuring the width of an emission line in a spectrum. An initial estimate of the outer limits of the redshift range of the cluster is made based on visual inspection of the pie diagrams (Fig. 1) and redshift histograms (Fig. 2). The redshift limits adopted are shown as dotted lines in Figures 1*b* and 2. A trial velocity dispersion, σ_1, is calculated using all the galaxies within the initial estimate of the redshift range. A second algorithm is used to assess the validity of this velocity dispersion in the presence of interlopers in the outer parts of the redshift space of the cluster. The velocity dispersion validation algorithm works as follows. The weighted (as in eq. [1]) velocities within $15\sigma_1$ (or the edge of the band-limiting filter if that is smaller) of the cluster center are put into bins $0.1\sigma_1$ wide (within reason the bin width has no effect). The mean density of the background in velocity space is calculated from the mean bin density more than $5\sigma_1$ away from the cluster. This background is then subtracted from the data within $3\sigma_1$ of the cluster center and the velocity dispersion σ_1' is calculated, along with a Bootstrap estimate of the error in σ_1'. If the 1 standard deviation confidence range for σ_1' includes σ_1 then it is accepted as the cluster's velocity dispersion; if not, then the redshift limits are further adjusted.

The adopted ranges in redshift, as defined by the above procedure, and field size, as defined by the rectangular region that bounds the data, are given in Table 1. Column (2) gives the weighted mean redshift, and columns (3) and (4) give the length and width of the bounding box in R.A. and decl. as converted to physical lengths, $D_A(z)\Delta\theta$, at the redshift of the cluster. The brightest cluster galaxy (BCG) is near the center of this box, but not exactly. Columns (5) and (6) give the lower and upper redshift boundaries. In Table 2 the second column gives the ratio of the "unlimited" σ_1' to the value accepted, and the third column gives the 1 standard deviation confidence interval for the σ_1'/σ_1 ratio. Each cluster's velocity dispersion is calculated using equation (1) with the weighted data in the cluster's redshift range given in Table 1. The results are given in Table 3. Column (2) of Table 3 is the redshift, and column (3) is the number of galaxies above the magnitude limit in the cluster R.A., decl. and redshift range. Column (6) is σ_1. The sky positions of the cluster galaxies for the inner 1000″ of the sample are shown in Figure 3.

The obvious redshift limits were acceptable in about half of the clusters. In the other half the limits were adjusted until a statistically acceptable result was found, or until no stable value emerged. The velocity dispersion checking algorithm indicates (Table 2) that the velocity dispersion of MS 0906+11 is significantly too large. No consistent solution could be found for this cluster, which appears to be an indistinct binary in redshift space. The other 15 clusters have velocity dispersions whose 1 or 2 standard deviation confidence ranges include the input velocity dispersion. Based on passing this test, the values in column (6) of Table 3 will be taken as our standard values. One could apply the slight corrections of Table 2, but that is simply changing the values within their standard error. The cluster MS 1358+62 has a common velocity group on its southern side, but this is not large enough to significantly disturb its rms velocity dispersion and is left in the sample. The mean value of σ_1'/σ_1, excluding MS 0906+11, is 0.986 ± 0.021.

The modified mean harmonic radii, R_h, are calculated for each cluster using the entire angular extent of the available data in the redshift range of the cluster as fixed for the σ_1 calculation. The angular extent of the clusters is defined by the angular limits on the sky of our sample. The resulting r_v are given in column (4) of Table 3.

1996ApJ...462...32C

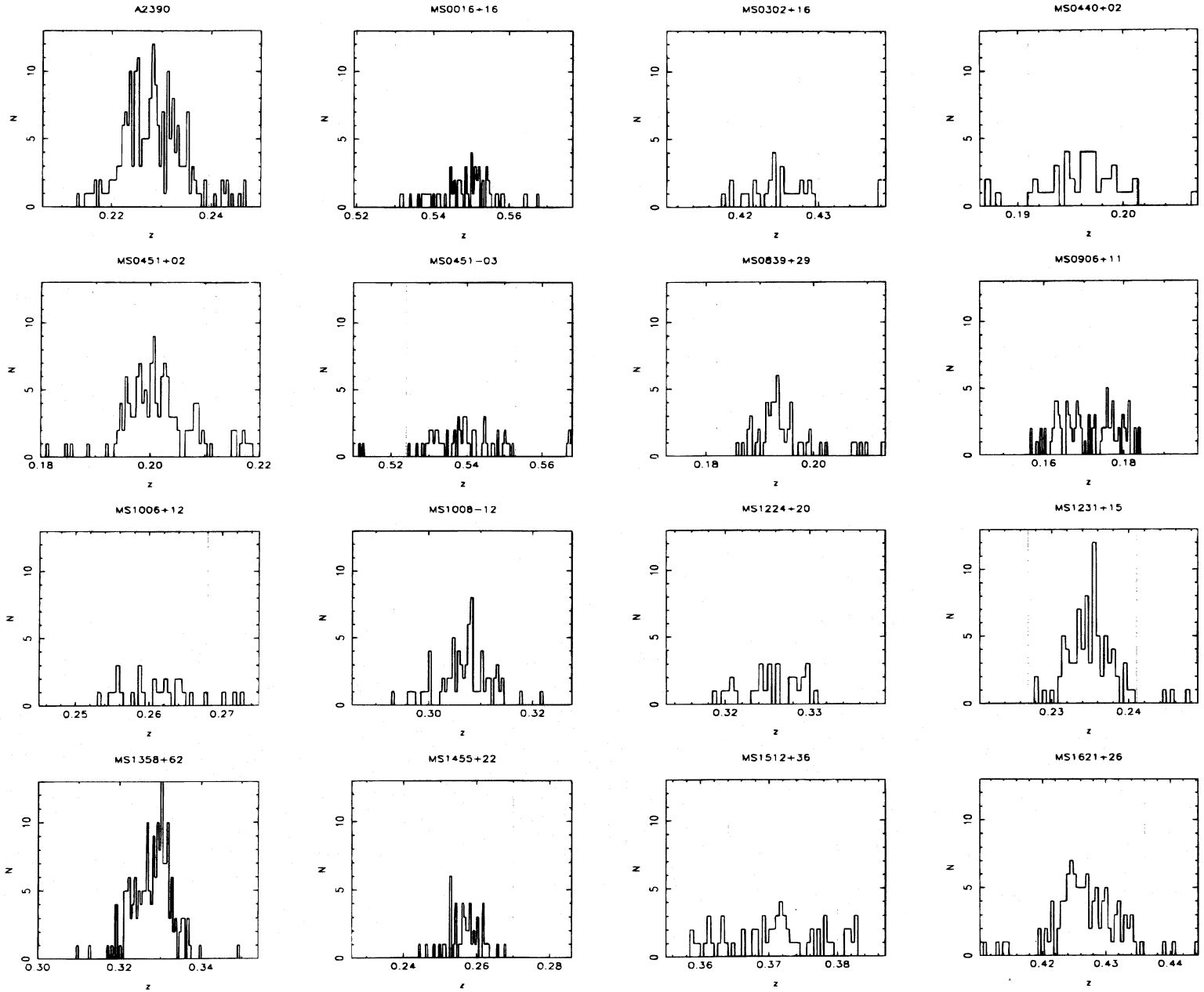

FIG. 2.—Redshift histograms in the vicinity of the clusters. The dashed lines indicate the selected cluster redshift range.

TABLE 1

CLUSTER REDSHIFT AND FIELD LIMITS

Name (1)	z (2)	R.A. (h^{-1} Mpc) (3)	Decl. (h^{-1} Mpc) (4)	z_{lo} (5)	z_{hi} (6)
A2390	0.2279	6.13	1.11	0.2175	0.2395
MS 0016+16.....	0.5466	2.19	1.87	0.5300	0.5587
MS 0302+16.....	0.4246	1.94	1.73	0.4160	0.4300
MS 0440+02.....	0.1965	3.32	1.02	0.1910	0.2013
MS 0451+02.....	0.2010	4.52	1.57	0.1919	0.2120
MS 0451−03.....	0.5392	2.26	1.87	0.5240	0.5530
MS 0839+29.....	0.1928	3.37	0.96	0.1820	0.2024
MS 0906+11.....	0.1709	1.06	0.86	0.1567	0.1838
MS 1006+12.....	0.2605	1.43	1.20	0.2530	0.2680
MS 1008−12.....	0.3062	1.61	1.36	0.2934	0.3144
MS 1224+20.....	0.3255	1.66	1.35	0.3180	0.3310
MS 1231+15.....	0.2350	1.34	3.16	0.2270	0.2410
MS 1358+62.....	0.3290	1.72	4.27	0.3150	0.3420
MS 1455+22.....	0.2570	1.47	1.21	0.2400	0.2700
MS 1512+36.....	0.3726	5.51	1.70	0.3640	0.3800
MS 1621+26.....	0.4274	2.04	5.15	0.4190	0.4360

It is expected (Gott & Gunn 1972) and borne out by numerical simulation (see, e.g., Crone, Evrard, & Richstone 1994) that, on the average, substantially all the virialized cluster mass is contained inside the radius where $\bar{\rho} > 200\rho_c$.

TABLE 2

VELOCITY DISPERSION VALIDATION

Name	σ_1'/σ_1	1 Standard Deviation Interval
A2390	1.07	0.99–1.11
MS 0016+16.....	1.07	0.93–1.15
MS 0302+16.....	0.96	0.77–1.09
MS 0440+02.....	0.95	0.60–1.14
MS 0451+02.....	0.85	0.67–0.98
MS 0451−03.....	0.96	0.84–1.01
MS 0839+29.....	0.93	0.55–1.10
MS 0906+11.....	0.37	0.22–0.49
MS 1006+12.....	0.93	0.74–1.00
MS 1008−12.....	1.03	0.90–1.09
MS 1224+20.....	0.97	0.85–1.04
MS 1231+15.....	1.04	0.95–1.10
MS 1358+62.....	0.96	0.91–1.02
MS 1455+22.....	0.97	0.85–1.09
MS 1512+36.....	1.18	1.00–1.32
MS 1621+26.....	0.92	0.83–1.00

Outside that radius, the velocities very rapidly become dominated by infall. Therefore, the ratio $\bar{\rho}(r_v)/\rho_c$ is used as a test of the completeness of the radial extent of the sampling of the cluster. This ratio is calculated as the mean density inside r_v to the critical density at the observed redshift by dividing the virial mass (eq. [4]) by the volume inside r_v:

$$\frac{\bar{\rho}(r_v)}{\rho_c(z)} = \frac{1}{\rho_c(z)}\frac{3M_v}{4\pi r_v^3} = \frac{6}{(1+z)^2(1+\Omega_0 z)}\frac{\sigma_1^2}{H_0^2 r_v^2}. \quad (5)$$

The critical density at redshift z is $\rho_c(z) = \rho_c(0)(1+z)^2(1+\Omega_0 z)$, which for $\Omega_0 = 1$, has the $(1+z)^3$ dependence of the mean density. For $\Omega_0 < 1$ equation (5) means that the density ratio at z is somewhat larger than for $\Omega_0 = 1$, with the difference being 25% at $z = \frac{1}{3}$ for our adopted $2q_0 = \Omega_0 = 0.2$.

The *total* virialized mass of the cluster should be accurately estimated if the mean density inside r_v is $200\rho_c$ or less. Table 3 includes nine clusters for which this criterion is met (see discussion below). For reference, the Coma cluster has $R_h \simeq 1.78\ h^{-1}$ Mpc (1°48, Schwarzschild 1954, or ZCAT

TABLE 3

CNOC CLUSTER DYNAMICAL PARAMETERS

Name (1)	z (2)	N (3)	r_v (h^{-1} Mpc) (4)	ϵ_r (h^{-1} Mpc) (5)	σ_1 (km s^{-1}) (6)	ϵ_σ (km s^{-1}) (7)	$\bar{\rho}(r_v)/\rho_c(z)$ (8)
A2390	0.2279	178	3.156	0.24	1093	61	46
MS 0016+16.....	0.5466	47	1.569	0.19	1234	128	140
MS 0302+16.....	0.4246	27	0.833	0.20	646	93	164
MS 0440+02.....	0.1965	36	1.994	0.27	606	62	37
MS 0451+02.....	0.2010	113	2.316	0.27	988	76	73
MS 0451−03.....	0.5392	51	1.407	0.17	1371	105	217
MS 0839+29.....	0.1928	44	0.929	0.23	749	104	264
MS 0906+11.....	0.1709	81	0.930	0.05	1893	113	1753
MS 1006+12.....	0.2605	26	1.028	0.10	906	101	279
MS 1008−12.....	0.3062	67	0.912	0.07	1054	107	443
MS 1224+20.....	0.3255	24	0.785	0.25	802	90	335
MS 1231+15.....	0.2350	74	1.519	0.14	667	69	72
MS 1358+62.....	0.3290	164	2.307	0.20	937	54	53
MS 1455+22.....	0.2570	50	1.021	0.07	1133	140	445
MS 1512+36.....	0.3726	38	1.665	0.68	690	96	51
MS 1621+26.....	0.4274	98	2.254	0.23	793	55	34

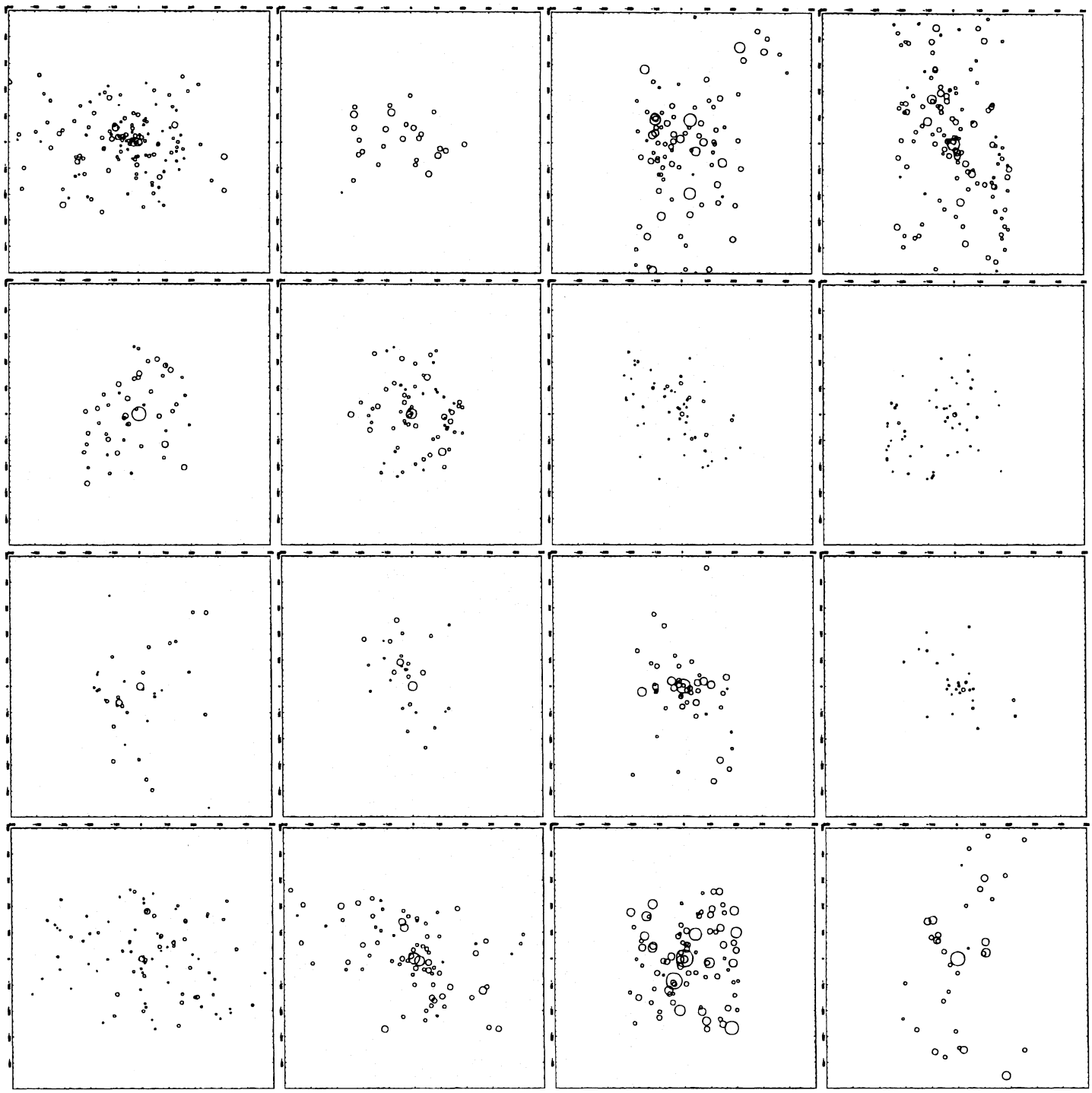

FIG. 3.—Sky locations of the galaxies in the redshift range of the cluster. The circle area is proportional to the galaxy's apparent magnitude. Each box is 1000″ on a side. The same layout of the clusters as in Figures 1, 2, and 3 is used. North is at the top, and east is to the left.

data, Huchra et al. 1992, with velocity cuts at ± 3000 km s^{-1} and within a 3° circle gives 1°.50) and, taking σ_1 to be 1040 km s^{-1} (Peebles 1970), has $\bar{\rho}(r_v) = 77\rho_c$. The local density at the outer edge of the sample clusters is no greater than $\frac{1}{3}\bar{\rho}(r_v)$, so for the clusters with $\bar{\rho}(r_v) \sim 50$, the local overdensity will only be $\sim 20\rho_c(z)$. This however, is greater than the turnaround density.

3.2. *Error Analysis*

The errors in σ_1, R_h, M_v, and M_v/L are assessed using the Jacknife technique. This is one of the simplest resampling techniques, wherein partial standard deviations, δ_i, are calculated by taking the difference between the $f(x_1, \ldots, x_n)$, where f is any statistical quantity calculated from the data set, and the same quantity calculated dropping one element at a time of the data set, $\delta_i = f(x_1, \ldots, x_n) - f(x_1, \ldots, x_{i-1}, x_{i+1}, \ldots, x_n)$. The estimate of the variance is $[n/(n-1)\sum_i \delta_i^2]^{1/2}$ (Efron 1981; Efron & Tibshirani 1986). For a Gaussian distributed sample the Jacknife variance converges to the normal value. A closely related technique is the Bootstrap, in which randomly drawing *with replacement* from the original data set creates many new data sets

of the same size as the original, which are then analyzed in precisely the same manner as the original to give a distribution of results from which confidence intervals are calculated. A significant difference is that the Bootstrap data sets have repeated values, which for pairwise statistics gives singularities. Also, the Bootstrap can be computationally quite expensive, since tests indicate (Efron & Tibshirani 1986) that 300 or more resamplings are required to give solid results. The errors given in Table 3 (in the columns labeled ϵ_r and ϵ_σ) are approximately in accord with a $N^{1/2}$ expectation but have significant differences in detail. The reliability of these errors is extremely important for one of the major results of this paper. We believe the pragmatic nature of the Jacknife error estimate is well suited to the task.

3.3. *Sample Commentary*

A cluster-by-cluster comparison with the results of other workers is done in the data papers for each cluster. In a number of cases our velocity dispersions are notably lower than those previously found. For instance, we find for Abell 2390 that $\sigma_1 = 1100 \pm 63$ km s^{-1}, whereas a previous study in the central region found 2112^{+274}_{-197} km s^{-1} (Le Borgne et al. 1991). In general the differences from previous work can be attributed to three factors. First, the precision of our velocities, $\simeq 100$ km s^{-1}, reduces catastrophic velocity errors and helps identify significant substructures. Second, our data cover a large radial range in the cluster, which makes them less subject to local substructure, and more representative of the rms value. Third, the bluer galaxies, which often contain measurable emission lines, statistically are found to have a higher velocity dispersion than the redder absorption line galaxies, an effect that is particularly prominent near the projected center of the cluster (Abraham et al. 1996; Carlberg et al. 1996a). Since redshifts are easily measured from emission lines, this can lead to an upward bias in the velocity dispersion, but which is demonstrated to be quite small in our data (YEC). These effects lead to even larger errors in the presence of substructure, for which there is evidence in many of our clusters. In general the CNOC clusters are quite regular, possibly a consequence of their high X-ray luminosity, and therefore substructure does not compromise any of the results below. The prime exception is MS 0906+11, which is removed from all averages.

The quantity $\bar{\rho}(r_v)$ in Table 3 varies from a low of $34\rho_c(z)$ in MS 1621+26 to a high of $445\rho_c(z)$ in MS 1455+22, discounting MS 0906+11. It is clear that $\bar{\rho}(r_v)$ is high for those clusters for which only a central field was observed. In particular, we expect on the basis of Coma data and n-body simulations, that it is necessary (but not sufficient) that $\bar{\rho}(r_v)$ should be less than $200\rho_c$ if the formal M_v (eq. [4]) is interpreted as the total virialized mass. If $\bar{\rho}(r_v) > 200\rho_c$ then it indicates that r_v is an underestimate of the true value for the entire virialized system, which is a straightforward consequence of the limited angular sampling of some of our clusters. This undersampling, when it occurs, does not compromise the major goals of this project, as shown below.

4. VIRIAL MASS ANALYSIS

The quantities σ_1 and r_v are given in Table 3. The resulting M_v-values, derived using equation (4) in units of solar masses, are given in Table 4 in column (3), with column (2) repeating the $\bar{\rho}(r_v)$ column of Table 3. It must be borne in mind that the masses given are defined by the radial extent of the sample and must be referred to the mean density given in column (2). That is, if the cluster extends beyond the size of our observed field, our mass is an underestimate of the total mass. Nevertheless, it remains of considerable interest to compute an M_v/L for the part of the cluster we observe. Furthermore, it is relatively straightforward to bring all the masses to a common ground.

The virial mass, as calculated from a data set missing the outer parts of the cluster, will still accurately estimate the mass contained within the orbits of the galaxies observed, with a weak dependence on the radial extent of the sampling as we show here. The virial theorem is derived by multiplying the Jeans equation of stellar "hydrostatic" equilibrium (a vector equation) with coordinate vectors and integrating over the volume of the system (see, e.g., Binney & Tremaine 1987). The outer limit of the volume integral is usually taken at infinity, but, when evaluated for a finite subset of the entire volume, gives an additional term to be evaluated at the outer surface. The scalar virial theorem for

TABLE 4

CNOC CLUSTER M_v AND L

Name (1)	$\bar{\rho}(r_v)/\rho_c(z)$ (2)	M_v ($h^{-1} M_\odot$) (3)	L ($h^{-2} L_\odot$) (4)	M_v/L ($h\, M_\odot\, L_\odot^{-1}$) (5)	$\epsilon_{M/L}$ ($h\, M_\odot\, L_\odot^{-1}$) (6)	M_{200} ($h^{-1} M_\odot$) (7)	L_{200} ($h^{-1} L_\odot$) (8)
A2390	46	2.6×10^{15}	7.8×10^{12}	331	54	1.2×10^{15}	3.7×10^{12}
MS 0016+16	140	1.6×10^{15}	6.5×10^{12}	254	79	1.3×10^{15}	5.4×10^{12}
MS 0302+16	164	2.4×10^{14}	9.6×10^{11}	248	107	2.2×10^{14}	8.7×10^{11}
MS 0440+02	37	5.0×10^{14}	1.2×10^{12}	420	120	2.2×10^{14}	5.2×10^{11}
MS 0451+02	73	1.6×10^{15}	3.3×10^{12}	475	89	9.7×10^{14}	2.0×10^{12}
MS 0451−03	217	1.8×10^{15}	4.5×10^{12}	406	100	1.9×10^{15}	4.7×10^{12}
MS 0839+29	264	3.6×10^{14}	9.7×10^{11}	370	126	4.1×10^{14}	1.1×10^{12}
MS 0906+11	1753	2.3×10^{15}	2.0×10^{12}	1148	245	6.8×10^{15}	5.9×10^{12}
MS 1006+12	279	5.8×10^{14}	1.5×10^{12}	382	121	6.9×10^{14}	1.8×10^{12}
MS 1008−12	443	7.0×10^{14}	2.2×10^{12}	312	84	1.0×10^{15}	3.3×10^{12}
MS 1224+20	335	3.5×10^{14}	1.3×10^{12}	261	137	4.5×10^{14}	1.7×10^{12}
MS 1231+15	72	4.6×10^{14}	1.9×10^{12}	250	63	2.8×10^{14}	1.1×10^{12}
MS 1358+62	53	1.4×10^{15}	5.9×10^{12}	236	31	7.2×10^{14}	3.0×10^{12}
MS 1455+22	445	9.0×10^{14}	1.1×10^{12}	807	260	1.3×10^{15}	1.6×10^{12}
MS 1512+36	51	5.5×10^{14}	1.4×10^{12}	376	228	2.8×10^{14}	7.1×10^{11}
MS 1621+26	34	9.8×10^{14}	5.5×10^{12}	178	39	4.0×10^{14}	2.3×10^{12}

a spherically symmetric system bounded at radius r_b becomes

$$\int_0^{r_b} (\sigma_r^2 + 2\sigma_\theta^2)\rho\, dV + \int_0^{r_b} \frac{-GM(r)}{r}\,\rho\, dV = 4\pi\rho\sigma_r^2 r_b^3 . \quad (6)$$

The right-hand side of equation (6) is sometimes called the $3PV$ surface term. The effect of ignoring the surface term for a gravitating system is to overestimate the mass of the system, since the surface pressure reduces the amount of mass to keep the system in equilibrium.

A singular isothermal sphere gives an estimate of the largest fractional error in the virial mass, equation (4), given a partially sampled cluster. The isothermal sphere provides an upper limit, since equilibrium stellar systems normally have a falling velocity dispersion with radius, so the isothermal sphere has an unusually large surface term. The density profile of a singular, isotropic, isothermal sphere of velocity dispersion $\sigma = \sigma_r$ is $\rho = (2\pi G)^{-1}\sigma^2 r^{-2}$. Equation (6) then becomes

$$3\sigma^2 M_b - \frac{GM_b^2}{r_b} = \sigma^2 M_b , \quad (7)$$

where M_b is the mass inside the boundary. If the surface term is neglected, then the derived virial mass will be an overestimate of the mass contained inside r_b, $3G^{-1}\sigma^2 r_b$, instead of the correct $2G^{-1}\sigma^2 r_b$. If the density profile declines more rapidly than r^{-2}, as is indeed the case for the clusters studied here (Carlberg et al. 1996a), then the error introduced through the neglect of the surface term is reduced. The isothermal sphere has the pleasing property that the relative size of the surface term is completely independent of shape or size of the surface. We conclude that if only an inner part of the cluster profile is sampled, then the calculation of the virial mass will be at most a 50% overestimate.

Under the assumption that clusters are approximately $\rho(r) \propto r^{-2}$ (or any other mass profile of interest), the masses can then be cautiously extrapolated to other radii or mean interior densities. The results of extrapolating the masses to a constant mean interior density of $200\rho_c$ using $M_{200} = M_v[\bar{\rho}(r_v)/(200\rho_c)]^{1/2}$ are given in the second to last column of Table 4.

In "raw" M_v the most massive cluster in the sample is A2390 (discounting MS 0906+11), with $M_v = 2.6 \times 10^{15}\ h^{-1}\ M_\odot$, which makes it more massive than Coma's $2.1 \times 10^{15}\ h^{-1}\ M_\odot$. A2390 and Coma have mean interior overdensities at r_v of 46 and 77, respectively, giving them nearly equal M_{200}-values of 1.2 and $1.3 \times 10^{15}\ h^{-1}\ M_\odot$, respectively. The masses of the other clusters range a factor of about 2.5 bigger and smaller than $M_{200} \sim 5 \times 10^{14}\ h^{-1}\ M_\odot$. This rather narrow range in mass is a consequence of our X-ray luminosity and flux selection. It is perhaps not too surprising that one of the most massive clusters, MS 0016+16, is also the highest redshift one in our sample.

5. CLUSTER GALAXY LUMINOSITIES AND NUMBERS

There are two practical approaches to relate empirically the cluster contents to a comoving volume in the field: the total luminosity of the cluster, and the number of cluster galaxies brighter than a certain absolute-magnitude limit. A third approach, a total cluster baryon inventory (White et al. 1993), cannot at present directly relate the cluster to the field, since most field baryons are in some unobserved form and one must turn to the Big Bang Nucleosynthesis argument (see, e.g., Walker et al. 1991) to obtain a field density of the baryons. However, the large reservoir of nonstellar baryons in clusters raises concern about the assumption that the fractional conversion of gas into stars has been the same in clusters and the field. Our galaxy sample extends from cluster to the far field, allowing a number of tests for variation. The "binary" cluster, MS 0906+11 is excluded from all averages calculated below.

The total luminosity of a cluster estimates the comoving volume from which it collapsed, $V = L/j$. This approach assumes that the total luminosity is conserved, or that any systematic change in galaxy luminosities during the gravitational assembly of the cluster can be measured and corrected. However, the subject of galaxy evolution within clusters remains quite controversial, at the very least because the observational phenomena are not yet well defined.

An alternate approach to measuring the equivalent field comoving volume of the cluster is to use the numbers of cluster galaxies above some absolute magnitude in ratio to the field, $V = \rho_c/\Phi(>L)$. Each of these methods has different strengths and weaknesses, but they are substantially *independent* since cluster total luminosities are dominated by the brightest galaxies but the total numbers are dominated by the low-luminosity galaxies. One possible evolutionary effect is the merging of the stellar components of two galaxies, which makes no difference to the total luminosity if there is no accompanying episode of star formation. Merging does, of course, decrease the numbers of galaxies. It is well known that cluster galaxies are on average significantly redder than field galaxies (Fig. 4), which is taken to indicate that star formation has decreased in cluster galaxies and hence they are less luminous per unit stellar mass than in the field. Fading will decrease the numbers of cluster galaxies above some fixed luminosity limit relative to the field, although, if the limit is well below M_*, then the decreased numbers will be a small fraction of the change in luminosity. For instance, if all cluster galaxies down to $M_r^K = -18.5$ mag were included in the total count, but there had been a 1 mag fading with respect to the field, then galaxies down to -17.5 mag should have been included in the total count. The expected increase in numbers (for a Schechter function with $M_* = -20.3$ mag and $\alpha = 1.10$) would be only 16%, as compared to a 150% correction required to the luminosity. Cluster galaxies are not simply post–star formation field galaxies with diminished luminosities, since clusters contain a population of very luminous, but very red, elliptical and cD galaxies in their centers. These may have been created through mergers, or they could have tapped the large baryon reservoir present in the cluster to create more stars. If galaxy luminosities are either increased or decreased, the L of a cluster responds in proportion, but the numbers of cluster galaxies above some magnitude change far less. The evolution of cluster galaxies relative to field galaxies, especially at these redshifts, is sufficiently ill defined that we do not, at this stage, want to make a highly uncertain differential correction. However, we will use mass-to-light and mass per galaxy to obtain two substantially independent estimates of Ω, which in turn will be used to address the notoriously difficult problem of constraining the size of systematic errors. That is, if the two estimators give discrep-

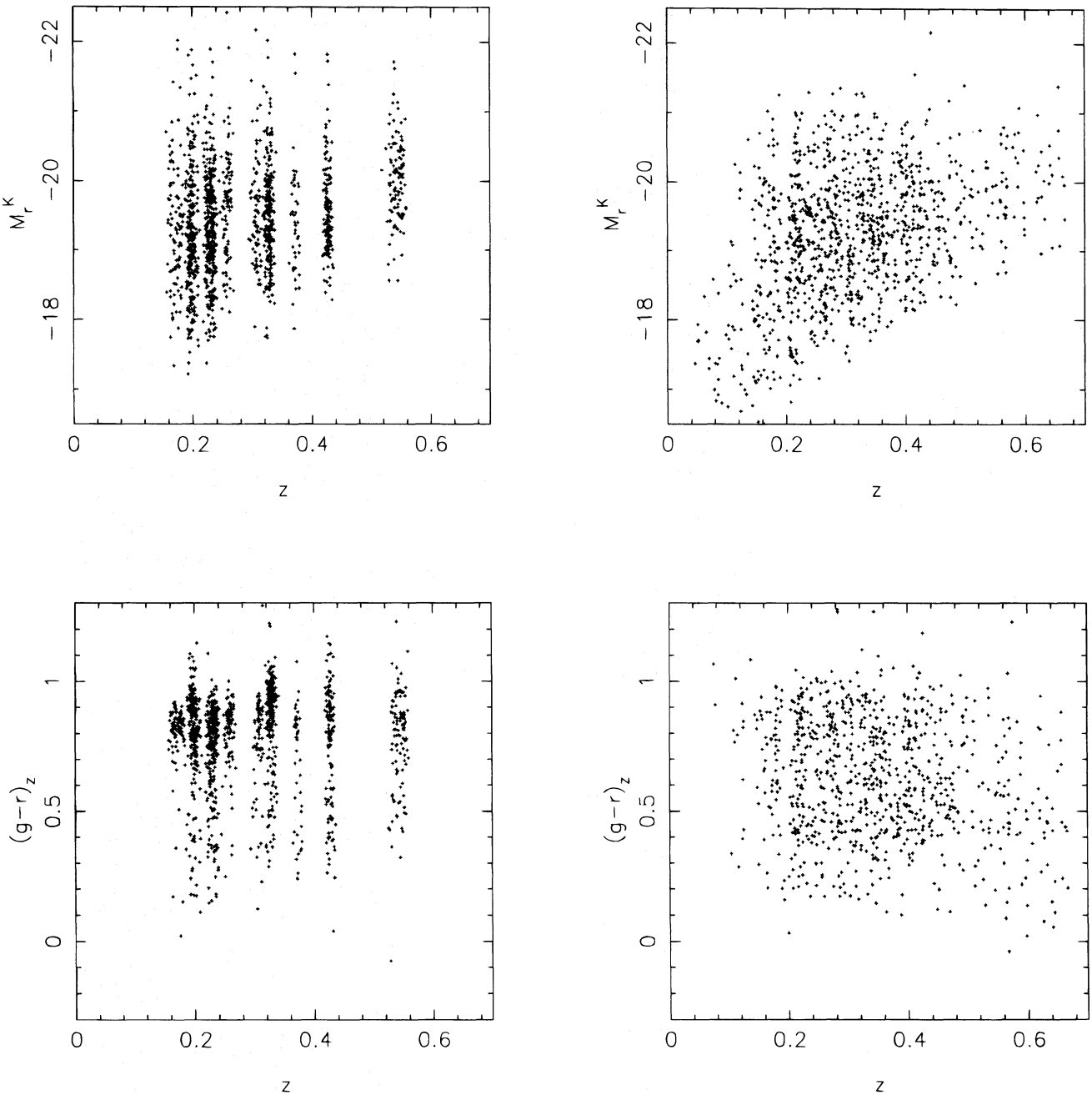

FIG. 4.—Corrected luminosities (*top row*) and normalized colors (*bottom row*) for cluster galaxies (*left column*) and field galaxies (*right column*).

ant values beyond the errors, then we would have detected a systematic effect (whose source would then be identified and corrected, if possible). We cannot empirically detect systematic errors smaller than our random errors, which then become our systematic error estimate.

The observed luminosity of the cluster galaxies, summed to $M_r^K = -18.5$ mag, corrected as described below, is reported in Table 4. The luminosity is measured in the Gunn r band, using $M_r(\odot) = 4.83$ mag. We also note that r band selection has the useful benefit that it is not unduly sensitive to star formation increases, although these are readily detected in the $g - r$ colors. The measured m_r are K-corrected using the following method. Model K-corrections in r and $g - r$ colors as a function of redshift for nonevolving galaxies of four spectral types (E+S0, Sbc, Scd, and Im) are derived by convolving filter response functions with spectral energy distributions from Coleman, Wu, & Weedman (1980). These values are then corrected from the AB system to the standard Gunn system (Thuan & Gunn 1976). For each galaxy with redshift, a color classification is estimated by comparing the observed $g - r$ color with the model colors at the same redshift. The spectral classification, obtained via interpolation, is treated as a continuous variable within the four spectral types. From the spectral classification, the appropriate K-correction to the r-magnitude is then derived using the models. No luminosity evolution correction is applied, but its possible effects are discussed below (see § 6).

It is conventional to quote M_v/L-values that are based on the "total light," that is, a correction is made for the part of the luminosity function below the limiting magnitude. This is not strictly necessary here, since the field sample is treated

in precisely the same manner, but for the sake of comparability, whenever galaxy luminosities are summed, they, both cluster and field, are *always* multiplied by a correction factor, ~15% as calculated below, to give "total luminosities." The correction for galaxies fainter than the limiting magnitude of our sample assumes $M_* = -20.3 + 5 \log h$ mag and $\alpha = -1.10$ in a Schechter luminosity function, $\phi(L) = (L/L_*)^\alpha \exp[-L/L_*]$. Our standard absolute-magnitude limit is $M_r^K = -18.5$ mag, which is about $0.2L_*$, unless explicitly stated otherwise. For the calculation of M_v/N, the numbers of galaxies are normally counted to this limit, with no correction for less luminous objects.

The K-corrected magnitudes from which we estimate field and cluster luminosities and numbers are shown in Figure 4. The M_v/L ratio and its standard error from the Jacknife technique are presented in columns (5) and (6), respectively, of Table 4. The M_v/N ratios derived using absolute-magnitude limits of $M_r^K = -18.5$ mag and -19.5 mag are given in columns (2) and (4), respectively, of Table 5. The errors of these quantities are in columns (3) and (5).

An entirely empirical redshift normalization of the colors, $(g-r)_z = (g-r)/[1.2 + 2.33(z - 0.3)]$, is also shown in Figure 4. This relation is based on a linear fit to the redshift dependence of the red sequence of the bright cluster galaxies. Because the median color of these clusters is always quite red, there is little range in the quantity $(g-r)_z$. The fraction of the galaxies that are blue can be estimated with a parameter similar, but quite different in detail, to the Butcher-Oemler blue fraction (Butcher & Oemler 1984). The quantity F_b here is the fractional weight of all galaxies in the cluster bluer than $(g-r)_z = 0.7$ mag. Note that this includes all galaxies used in the total luminosity and does not restrict the measurement of the blue fraction to some fiducial radius. A more detailed analysis of the Butcher-Oemler effect will be presented elsewhere (a preliminary account is in Yee et al. 1995c). The field galaxies are always substantially bluer than the cluster galaxies: the average $(g-r)_z$ is 0.55 mag, with no significant change with redshift over the entire range of $0.1 \le z \le 0.6$. The cluster galaxies have average $(g-r)_z$-values ranging from 0.72 mag to 0.94 mag. Although there is some overlap of the populations, there is no overlap of the averages. Hence, it is not possible to empirically estimate from this sample the luminosities of the cluster galaxies if they had the same color distribution as the field galaxies. Figures 5 and 6 show no significant dependence of the measured M_v/L and M_v/N on the colors or blue fraction of the cluster galaxy population, over the range of these clusters and given the errors in the measurements.

5.1. *Cluster Mass-to-Light Ratios*

It is immediately apparent from Table 4 and Figure 5 that the M_v/L do not show much variation outside their errors, in spite of the variations in the sampling radii. The variance weighted harmonic mean M_v/L for the sample as a function of limiting r-band absolute magnitude (always cor-

TABLE 5

CNOC CLUSTER M_v/N

Name (1)	$M_v/N(-18.5)$ ($h^{-1} M_\odot$) (2)	$\epsilon_{M/N}$ ($h^{-1} M_\odot$) (3)	$M_v/N(-19.5)$ ($h^{-1} M_\odot$) (4)	$\epsilon_{M/N}$ ($h^{-1} M_\odot$) (5)
A2390	3.2×10^{12}	4.9×10^{11}	6.1×10^{12}	1.0×10^{12}
MS 0016+16.....	9.5×10^{12}	2.9×10^{12}	9.5×10^{12}	2.9×10^{12}
MS 0302+16.....	3.2×10^{12}	1.2×10^{12}	3.2×10^{12}	1.2×10^{12}
MS 0440+02.....	5.1×10^{12}	1.3×10^{12}	8.9×10^{12}	2.8×10^{12}
MS 0451+02.....	5.0×10^{12}	7.8×10^{11}	1.1×10^{13}	2.4×10^{12}
MS 0451−03.....	1.4×10^{13}	3.3×10^{12}	1.4×10^{13}	3.4×10^{12}
MS 0839+29.....	3.7×10^{12}	9.9×10^{11}	7.7×10^{12}	2.6×10^{12}
MS 0906+11.....	1.4×10^{13}	2.6×10^{12}	2.8×10^{13}	6.7×10^{12}
MS 1006+12.....	8.6×10^{12}	2.8×10^{12}	8.6×10^{12}	2.8×10^{12}
MS 1008−12.....	4.6×10^{12}	1.2×10^{12}	6.0×10^{12}	1.9×10^{12}
MS 1224+20.....	4.6×10^{12}	2.3×10^{12}	5.0×10^{12}	2.7×10^{12}
MS 1231+15.....	2.8×10^{12}	6.7×10^{11}	4.4×10^{12}	1.3×10^{12}
MS 1358+62.....	3.0×10^{12}	3.8×10^{11}	4.3×10^{12}	5.7×10^{11}
MS 1455+22.....	9.1×10^{12}	2.5×10^{12}	1.6×10^{13}	6.2×10^{12}
MS 1512+36.....	4.9×10^{12}	3.0×10^{12}	1.0×10^{13}	4.6×10^{12}
MS 1621+26.....	3.4×10^{12}	6.7×10^{11}	3.4×10^{12}	7.0×10^{11}

TABLE 6

AVERAGE CLUSTER M_v/L AND M_v/N WITH SAMPLE ABSOLUTE-MAGNITUDE LIMIT

M_r^K	M_v/L ($h\, M_\odot\, L_\odot^{-1}$)	$\epsilon_{M/L}$ ($h\, M_\odot\, L_\odot^{-1}$)	M_v/N ($h^{-1} M_\odot$)	$\epsilon_{M/N}$ ($h^{-1} M_\odot$)
−18.0.....	309	61	3.9×10^{12}	1.1×10^{12}
−18.5.....	295	53	3.9×10^{12}	1.1×10^{12}
−19.0.....	265	42	4.2×10^{12}	1.1×10^{12}
−19.5.....	247	48	5.6×10^{12}	1.5×10^{12}
−20.0.....	212	47	8.9×10^{12}	2.4×10^{12}

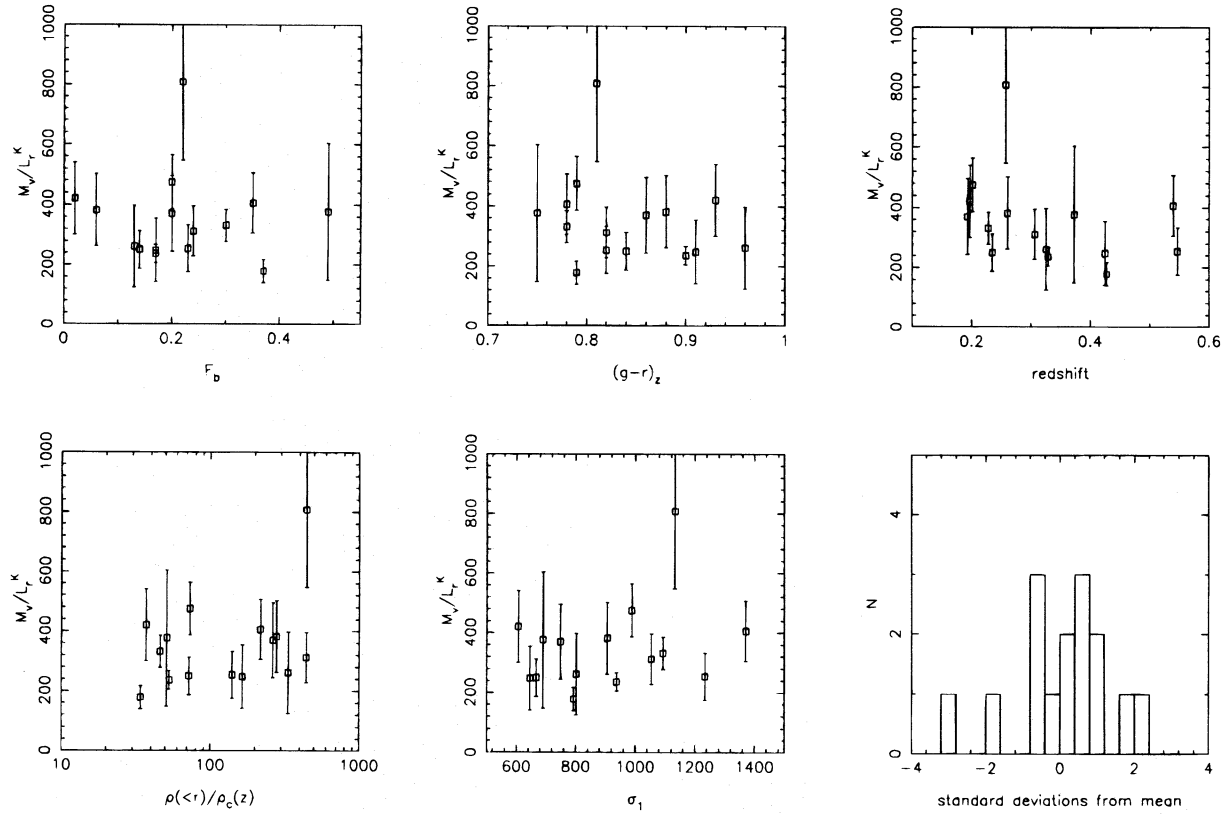

FIG. 5.—M_v/L ratio as a function of (*from left to right, top to bottom*) total blue fraction, color, redshift, mean interior density, and velocity dispersions, for $M_r^K = -18.5$ mag. The distribution of differences from the mean, ratioed to the estimated error, is in the lower right.

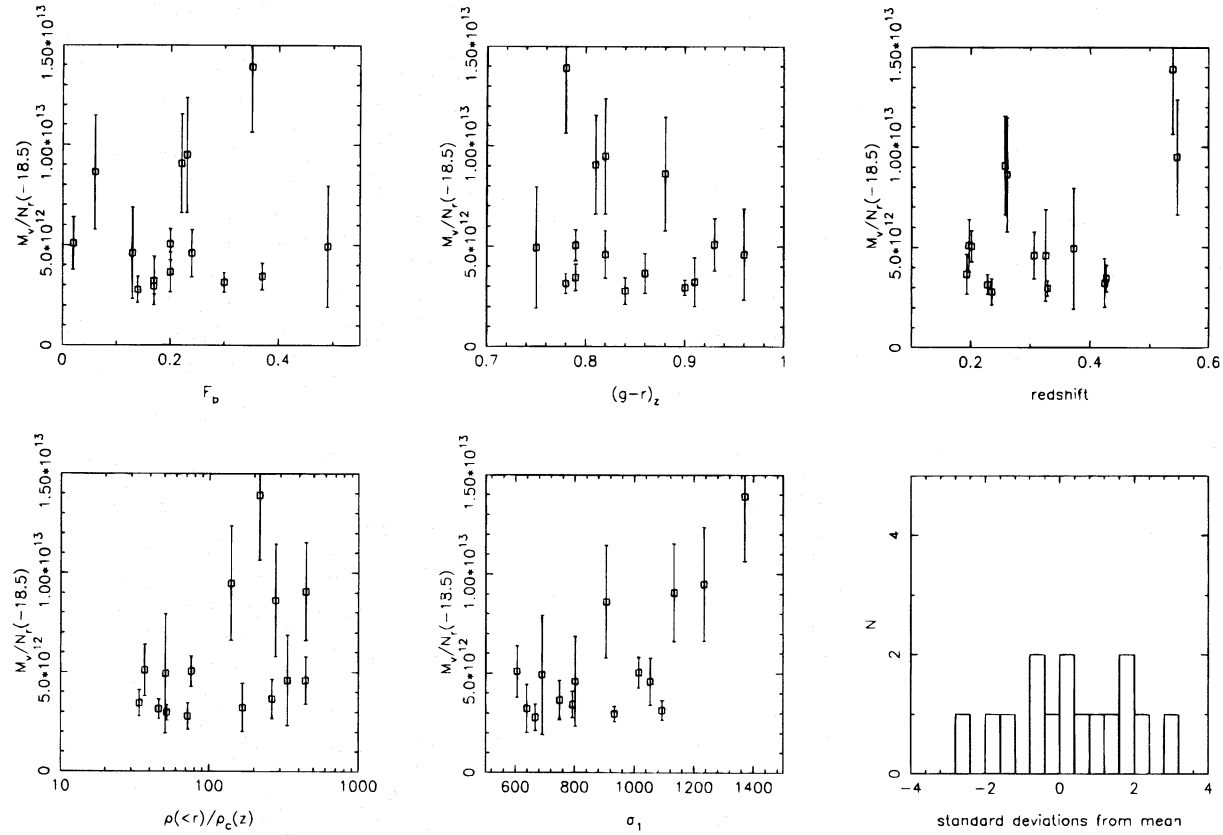

FIG. 6.—M_v/N ratio as a function of (*from left to right, top to bottom*) total blue fraction, color, redshift, mean interior density, and velocity dispersions, for $M_r^K = -18.5$ mag. The distribution of differences from the mean, ratioed to the estimated error, is in the lower right. The two highest redshift clusters are not complete to this limiting absolute magnitude and hence have erroneously large M_v/N-values.

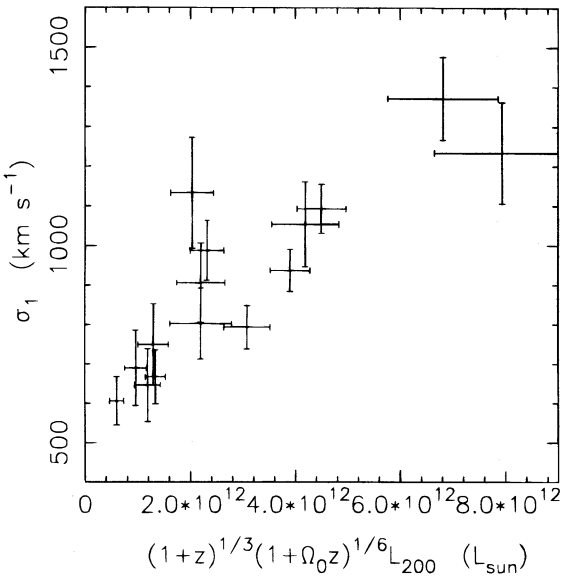

FIG. 7.—Constant overdensity luminosity plotted against the observed σ_1.

rected to total light as above) are given in Table 6. For $M_r^K = -18.5$ mag the mean M_v/L is $295 \pm 53\ h\ M_\odot\ L_\odot^{-1}$ (in Gunn r, with K-corrections). No luminosity evolution has been included. The M_v/L-values as a function of redshift are shown in Figure 5. No luminosity evolution has been included. The corrections to the luminosities are all multiplicative factors that are applied both to the field and the cluster data, so they have no effect on the Ω-value derived. No correlation between M_v/L and z, $\bar{\rho}(r_v)$ or σ_1 is apparent in Figure 5.

The distribution of M_v/L differences from the 15 cluster sample mean, normalized to their measurement errors, is also displayed in Figure 5. The cluster having a difference of -3.0 standard deviations, MS 1621+26, is one of the clusters with the best data and is also one of the bluer clusters. This possibly indicates that its luminosity is higher than it would be if the galaxies were allowed to age enough that the colors became comparable to other clusters in this redshift range. The redshift-M_v/L plot of Figure 5 also gives the impression that all the clusters have the same M_v/L (removing MS 0906+11) within the errors. The χ^2 per degree of freedom is 1.70, but removing MS 1621+26 as well reduces it to 1.18, which is consistent with no variation beyond the errors. That is, the M_v/L-values of Table 4 are consistent with a universal underlying M_v/L, after a 3 standard deviation clipping is applied. This means that the measured cluster light is a very good indicator of the mass contained within the orbits of the galaxies. However, the case of MS 1621+26 likely indicates that we are near the limit of detecting real cluster to cluster variations resulting from differences in galaxy population mix. It is intriguing to note that this appears to be true over a substantial range of mean interior densities that characterize the cluster samples. A similar result has been found for X-ray measurement of cluster masses (David et al. 1995), although their M/L profiles decline with increasing overdensity, whereas our integrated values are nearly constant, or rise slightly, with mean interior overdensity, within the limits expected from the virial surface term of equation (7).

The percentage errors in the M_v/L-values are in the 10%–30% range, depending on the number of cluster galaxies. With more data, it seems quite likely that it will become evident that there are intrinsic variations in cluster M_v/L-values. In particular the cluster light could have a "second-order" luminosity correction, which would depend on the precise mix of galaxies in the cluster. Of course, any true M_v/L variations cannot be bigger than the error bounds found here.

5.2. *Cluster Mass-to-Number Ratios*

The mass per galaxy for all galaxies brighter than some chosen absolute magnitude is less sensitive to differential fading (or possible brightening) between the field and cluster than the mass per unit luminosity. Merging could alter the galaxy numbers, but, in as much as mergers lead to ellipticals (the E + A galaxies appear to be mostly disk systems; Dressler et al. 1994), it does not drastically alter the numbers of galaxies. Both fading and merging will cause the M_v/N ratio to overestimate the value of Ω. The individual mass-to-number ratios to a limiting magnitude of $M_r^K = -18.5$ mag are shown in Figure 6 and given to -18.5 and -19.5 mag in Table 5.

Figure 6 shows that M_v/N has no significant dependence on the blue fraction or mean color or redshift but weakly suggests an increase in scatter as a function of the mean interior overdensity. This is likely to be primarily a statistical effect, since the clusters with large $\bar{\rho}(r_v)$ are those where the sample does not extend to large radii. There is a tendency for the high-velocity dispersion clusters to have the largest M_v/N-values. Although this trend is not very significant, it is opposite to a standard biasing scheme, "peak-background," in which galaxy formation is initiated earlier and is more advanced in clusters of increasing mass.

The average values of M_v/N for all the clusters are given for a range of limiting absolute magnitudes in Table 6. The average M_v/N are calculated after dropping the two highest redshift clusters, MS 0451−03 and MS 0016+16, which are not complete to the fainter limiting absolute magnitudes, as well as the binary MS 0906+11. The mean value at $M_r^K = -19.0$ mag is $M_v/N = 4.2 \pm 1.1 \times 10^{12}\ h^{-1}\ M_\odot$. The χ^2 of the distribution of differences from the mean M_v/N, for a limit of -18.5 mag, is very large, about 3 per degree of freedom. At a limit of -20.0 mag MS 0451−03 and MS 0016+16 can be reinstated, and the χ^2 per degree of freedom drops to 1.12 if MS 1621+26 is dropped. Evidently, the M_v/N is much less stable than the M_v/L ratio, unless M_v/N is restricted to the bright galaxies, $L > L_*$, alone.

5.3. *The Luminosity-Velocity Dispersion Relation*

It is particularly interesting to check for correlations between dynamical quantities, such as σ_1, and relatively "cheap" observables such as the cluster luminosities. The luminosities must be put on a common basis, allowing for radial sampling and redshift variation, to check whether luminosity can be used to predict velocity dispersion. The luminosities can be extrapolated to a common mean density, L_{200}, in the same manner as the masses. That is, $L_{200} = L[\bar{\rho}(r_v)/(200\rho_c)]^{1/2}$, which is given in the last column of Table 4. We note that this builds in a correlation between L_{200} and $\sigma_1^{1/3}$, but it is not sufficient to explain the result below. The redshift dependence of L_{200} arises from the variation of ρ_c with z. That is, as a cluster of a given M_{200}, is moved to higher redshift it will become denser, hence its

velocity dispersion will increase. Basic scaling says $\sigma^2 \propto \rho^{1/3} M^{2/3}$, where $M \propto \rho r^3$ is used. With the redshift dependence of ρ included this becomes $\sigma_1 \propto (1+z)^{1/3} (1+\Omega_0 z)^{1/6} M^{1/3}$. Figure 7 plots L_{200} multiplied by the redshift factor against the velocity dispersion. This plot excludes MS 0906+11. The implication of Figure 7 is that an estimate of the total cluster light from an image will be a good predictor of its velocity dispersion. The accuracy of a practical technique to take advantage of this correlation will be discussed elsewhere.

6. LIGHT AND NUMBER DENSITIES OF FIELD GALAXIES

The closure mass-to-light ratio is defined as $(M/L)_c \equiv \rho_c/j$, where $\rho_c = 3H_0^2/(8\pi G)$, and $j = \int_0^\infty L\Phi(L)dL$, where $\Phi(L)$ is the field luminosity function. The integration is carried to low luminosities by assuming a Schechter form for the luminosity function for galaxies below the absolute-magnitude cutoff. Similarly, the closure $(M/N)_c \equiv \rho_c/\Phi(>L)$, where N_L is the number of galaxies more luminous than L. At low redshift $(M/L)_c$ is estimated to be about $1500^{+700}_{-400}\, h\, M_\odot\, L_\odot^{-1}$ (Efstathiou et al. 1988; Loveday et al. 1993). This value is based on a blue selected sample and integrates all the light in the luminosity function to very faint magnitudes. Our selection is based on Gunn r, and we do not sample galaxies much fainter than $M_r^K \simeq -18.5$ mag. These differences would lead to substantial systematic errors in Ω if we tried to ratio moderate redshift cluster light to a low-redshift field estimate of the closure density.

Our survey includes a built-in field sample that can be used to estimate accurately $(M/L)_c$ and $(M/N)_c$, on the same basis as our cluster values. Each field galaxy is K-corrected, and then within a redshift range we correct the total luminosity for light below our magnitude limit using precisely the same Schechter function parameters as used for the cluster galaxies. Because all of these factors are multiplicative, they cancel in the eventual ratio of interest, Ω. The corrections are done for the sake of providing numerical values having some degree of comparability to true low-redshift quantities. The luminosity density of the field can be nearly trivially calculated from our field sample, and offers the benefits that it is selected precisely the same, in the same filter band, in the same redshift range, and to the same limiting magnitude as the cluster data. This approach, using a self-consistent luminosity system for the cluster and field, greatly reduces concerns about systematic differences between the low-redshift estimate and our medium-redshift data.

Table 7 gives the results of the $(M/L)_c$ and $(M/N)_c$ calculation averaged over the redshift range $0.2 \le z \le 0.6$. The cluster redshift ranges of Table 1 are widened by $\Delta z = 0.01$ at both the upper and lower redshift to eliminate any concerns about an overestimate of j from a higher density of galaxies in the vicinity of these very rich clusters. In fact, there is no significant change in the field luminosity density without this extra cut around the clusters. The weighted luminosities of the field galaxies, corrected precisely the same as the cluster data, are simply summed in each redshift bin, cutting the sum off at various absolute magnitudes. The volumes are in *comoving* h^{-1} Mpc^3 integrated over the accessible redshift range of the bin for our chosen q_0, times the total solid angle accessible within each of the 16 cluster fields (as derived from a map in which bright stars, bad columns, and other inaccessible pixels are removed). The total effective field area covered is 2391 square arcmin. There is no statistically significant redshift trend between $z = 0.18$ and $z = 0.55$ in either the luminosity or number density in our K-corrected magnitude system. No luminosity evolution correction is applied over our redshift range, although there is a significant difference from the $z = 0$ luminosity function.

The random errors of our closure $(M/L)_c$ (col. [4] of Table 7) are calculated using the Jacknife technique assuming that each cluster field should be treated as a data element. This might be a conservative estimate of the errors, but it fully accounts for large-scale structure variations.

7. Ω

The value of Ω is estimated under the assumption that the M_v/L of the clusters is the same as M/L in the field. Our best estimate, in the sense of smallest random errors, uses data to $M_r^K = -18.5$ mag, which is corrected to total light using a Schechter function. We find $\Omega_z = 0.29 \pm 0.06$ at a mean redshift of 0.32. Brighter absolute-magnitude limits (similarly corrected to total light) use less data but give consistent values of Ω, with increased errors.

We have presented our results without an evolution correction, as the most direct approach. The field luminosity density has increased by a factor of 1.5 (in our data) relative to the $z = 0$ value of $\rho_c/j \simeq 1500\, h\, M_\odot\, L_\odot^{-1}$, but our measurement of Ω is done with respect to field galaxies in the same redshift range, so any correction done in common makes essentially no difference to the result. We have reanalyzed all results using luminosity evolutions of 1 and 2 mag per unit redshift, applied to both field and cluster galaxies, and find that the derived Ω changes no more than 0.2%. A differential evolution of the field and cluster population could make a significant change, depending on what redshift is chosen as the point of comparison. For instance, a match of our field luminosity density to the $z = 0$ value of $\sim 1500\, h\, M_\odot\, L_\odot^{-1}$ can be achieved with a luminosity evolu-

TABLE 7

THE CLOSURE M/L AND M/N-VALUES WITH SAMPLE ABSOLUTE-MAGNITUDE LIMIT

M_r^K (1)	ρ_c/j ($h\, M_\odot\, L_\odot^{-1}$) (2)	$\epsilon_{M/L}$ ($h\, M_\odot\, L_\odot^{-1}$) (3)	$\rho_c/\Phi(>L)$ ($h^{-1}\, M_\odot$) (4)	$\epsilon_{M/N}$ ($h^{-1}\, M_\odot$) (5)
−18.0.....	1114	153	1.35×10^{13}	3.5×10^{12}
−18.5.....	1025	140	1.35×10^{13}	3.5×10^{12}
−19.0.....	947	112	1.55×10^{13}	3.0×10^{12}
−19.5.....	846	85	1.91×10^{13}	3.1×10^{12}
−20.0.....	785	42	3.28×10^{13}	2.9×10^{12}

tion of about 1 mag per unit redshift, whereas our cluster data somewhat weakly indicate (in the $z > 0.4$ clusters) an evolution of about 2 mag per unit redshift. If our results were then corrected to $z = 0$ the derived Ω_z would be increased to 0.39 ± 0.10 from 0.29 ± 0.06. However, correcting to redshift zero makes little sense since that accentuates the color differences between the cluster and the field. Using precisely the same differential evolution and correcting to redshift $z \sim \frac{1}{3}$ gives a result essentially identical to our uncorrected Ω_z, and correcting to $z \simeq 0.55$, where the field and galaxy population begin to have substantial overlap of color, would lower Ω_z about 20%. We believe our current approach is the best, since both the clusters and the field galaxies with $z > 0.4$ do not contribute large numbers to the sample, and therefore are a small component of the variance weighted averages used for Ω_z.

The value of Ω_z from the M_v/N calculation is 0.27 ± 0.09 for absolute-magnitude limits of both $M_r^K = -18.5$ mag and -19.0 mag. This value is consistent with the one found from the M_v/L argument. We will prefer the M_v/L-value of Ω mainly because of its smaller errors, but also as the conventional approach. The fact that the M_v/L and the M_v/N routes to calculating Ω give similar results is considerable grounds for confidence in the result. The two Ω-values have substantially different dependencies on the evolution of cluster galaxies and are weighted to different parts of the luminosity function. Certainly, we would not be able to detect any systematic errors in cluster galaxy evolution, which is smaller than the quadrature summed random errors of the two Ω results. We will use this error sum as our estimate of the likely size of any residual systematic errors in our cluster Ω-values, due to galaxy evolution alone. It does not measure any systematic dynamical errors in the masses.

The M_v/L-values for the average cluster and the field (Tables 6 and 7) show a common trend, in that using fainter absolute-magnitude cutoffs (and hence, more real data) produces less total light when extrapolated via the adopted luminosity function. Although the trend is not significant, it is an indication that the adopted luminosity function (or the lack of an evolution correction) could be refined to better describe the data. As discussed above, this has an insignificant impact on Ω_z.

The current epoch $\Omega_0 = \Omega_z/[1 + z(1 - \Omega_z)]$, which at our average cluster redshift of 0.32 and for our measured $\Omega_z = 0.29 \pm 0.06$ gives $\Omega_0 = 0.24 \pm 0.05$, where the formal 1 standard deviation random error is given. The strength of this value is that it is based on our survey alone, which has well understood sampling statistics, needs no low-redshift comparisons and is done entirely within one photometric system requiring only small redshift corrections. The main issue that is addressed in companion papers is whether the virial mass correctly estimates the total mass of clusters, with further examination of the differences between cluster and field light per unit mass.

8. CONCLUSIONS

The CNOC cluster sample is a uniform, X-ray selected, sample of clusters having $0.17 < z < 0.55$. We derive velocity dispersions and a characteristic radius for each of these clusters, and calculate their virial mass, based upon objective tests to estimate the radial and redshift extent of the cluster members. The Gunn r-band luminosity of the clusters is K-corrected (but no evolution correction), and the ratio M_v/L to a limiting absolute magnitude of -18.5 mag, corrected to a total luminosity with a Schechter luminosity function, is found to have a mean value of $295 \pm 53\ h\ M_\odot\ L_\odot^{-1}$. The clusters are consistent with having identical M_v/L-values (for the corrected luminosities) within the sample variance, which is about 25%. Therefore, galaxy population and sampling variations have a small effect on M_v/L for our clusters.

The field luminosity density is calculated from the same data set so that we obtain an $(M/L)_c$ in the same redshift range. We find $(M/L)_c = 1025 \pm 140\ h\ M_\odot\ L_\odot^{-1}$, where the error is estimated from field-to-field variations. We conclude that the cluster virial masses universally indicate that $\Omega_z = 0.29 \pm 0.06$ for clusters at $z \simeq 0.32$, or $\Omega_0 = 0.24 \pm 0.05$. Our measurement of Ω is done completely within our data set, which diminishes many of the possible selection effects to small corrections to the luminosity, filter bands, and shape of the luminosity function, since they are done identically for the field and cluster galaxies. The concern that relative evolution of field and cluster galaxies could lead to systematic errors is partially constrained here and is addressed elsewhere (Abraham et al. 1996 and future papers). Cluster galaxies have largely ceased star formation, so if anything they are likely to be less luminous than field galaxies, meaning that the Ω given here is a likely somewhat of an overestimate. To constrain fading and merging of cluster galaxies, we measure the average M_v/N, which is $3.9 \pm 1.1 \times 10^{12}\ h^{-1}\ M_\odot$ to $M_r^K = -18.5$ mag and $4.2 \pm 1.1 \times 10^{12}\ h^{-1}\ M_\odot$ to $M_r^K = -19.0$ mag (excluding the binary MS 0906+11, and the high-redshift clusters MS 0016+16 and MS 0451−03, which are not well sampled to these luminosities). The closure M_v/N-values are nearly identical, but we take the brighter limit to find from M_v/N that $\Omega_z = 0.27 \pm 0.09$ or $\Omega_0 = 0.22 \pm 0.07$.

Within the errors the M_v/L and the M_v/N estimates for Ω are consistent with a single value, but, because relative evolution of the cluster and field galaxy population affects them differently, the sum squared errors in the two methods is used as an indicator of the systematic error resulting from the luminosity normalization, finding that it is 44%. We conclude that $\Omega_0 = 0.24 \pm 0.05 \pm 0.09$, which is completely incompatible with unity in a cold component. Differential galaxy fading between the cluster and field would reduce this value, although the reduction cannot be large because the M_v/L and M_v/N techniques (and our checks on the luminosity functions and color differentials between field and cluster) would then indicate a discrepancy beyond our errors.

Our self-contained technique eliminates many of the systematic errors of the M_v/L and M_v/N techniques for Ω estimation but leaves open the issue whether cluster galaxies are substantially more clustered than the cluster mass. This will be addressed with the same data set in a companion paper.

We thank all participants of the CNOC cluster survey for assistance in carrying out this project. Huan Lin and Mike Hudson provided valuable comments. The Canadian Time Assignment Committee for the CFHT generously allocated substantial grants of observing time, and the CFHT organization provided the technical support that made these observations feasible. We gratefully acknowledge financial support from NSERC and NRC of Canada.

REFERENCES

Abell, G. O. 1958, ApJS, 3, 211
Abraham, R. G., et al. 1996, AJ, submitted
Bahcall, N. A., Lubin, L. M., & Dorman, V. 1995, ApJ, 447, L81
Bahcall, J., & Tremaine, S. D. 1981, ApJ, 244, 805
Binney, J., & Tremaine, S. 1987, Galactic Dynamics (Princeton: Princeton Univ. Press)
Bird, C. M. 1995, ApJ, 445, 81
Bird, C. M., & Beers, T. C. 1993, AJ, 105, 1596
Butcher, H., & Oemler, A. 1984, ApJ, 285, 423
Carlberg, R. G. 1994, ApJ, 433, 468
Carlberg, R. G., et al. 1994, JRASC, 88, 39
Carlberg, R. G., Yee, H. K. C., & Ellingson, E. 1996a, preprint
Carlberg, R. G., et al. 1996b, preprint
Coleman, G. D., Wu, C., & Weedman, D. W. 1980, ApJS, 43, 393
Crone, M. M., Evrard, A. E., & Richstone, D. O. 1994, ApJ, 434, 402
David, L. P., Jones, C., & Forman, W. 1995, ApJ, 445, 578
Dressler, A. 1980, ApJ, 236, 351
Dressler, A., Oemler, A. J., Butcher, H. R., & Gunn, J. E. 1994, ApJ, 430, 107
Dressler, A., & Gunn, J. E. 1983, ApJ, 270, 7
Efron, B. 1981, Biometrika, 68, 589
Efron, B., & Tibshirani, R. 1986, Statistical Science, 1, 54
Efstathiou, G., Ellis, R. S., & Peterson, B. A. 1988, MNRAS, 232, 431
Gioia, I. M., & Luppino, G. A. 1994, ApJS, 94, 583
Gioia, I. M., Maccacaro, T., Schild, R. E., Wolter, A., Stocke, J. T., Morris, S. L., & Henry, J. P. 1990, ApJS, 72, 567
Gott, J. R., & Gunn, J. 1972, ApJ, 176, 1
Gunn, J. E. 1978, in Observational Cosmology, ed. A. Maeder, L. Martinet, & G. Tammann (Sauverny: Geneva Obs.), 1
Henry, J. P., Gioia, I. M., Maccacaro, T., Morris, S. L., Stocke, J. T., & Wolter, A. 1992, ApJ, 386, 408
Huchra, J. P., Geller, M. J., Clemens, C. M., Tokarz, S. P., & Michel, A. 1992, The CfA Redshift Catalogue ZCAT, Bull. Inf. CDS 41
Kent, S., & Gunn, J. E. 1982, AJ, 87, 945
Le Borgne, J. F., Mathez, G., Mellier, Y., Pello, R., Sanahuga, B., & Soucail, G. 1991, A&AS, 88, 133
LeFèvre, O., Crampton, D., Felenbok, P., & Monnet, G. 1994, A&A, 282, 340
Limber, D. N. 1959, ApJ, 130, 414
Limber, D. N., & Mathews, W. G. 1960, ApJ, 132, 286
Loveday, J., Efstathiou, G., Peterson, B. A., & Maddox, S. J. 1993, ApJ, 390, 338
Peebles, P. J. E. 1970, AJ, 75, 13
Plionis, M., Barrow, J. D., & Frenk, C. S. 1991, MNRAS, 249, 662
Press, W. H., Teukolsky, S. A., Vetterling, W. T., & Flannery, B. P. 1992, Numerical Recipes in C (Cambridge: Cambridge Univ. Press)
Ramella, M., Geller, M. J., & Huchra, J. P. 1989, ApJ, 344, 57
Rood, H. J., Page, T. L., Kintner, E. C., & King, I. R. 1972, ApJ, 175, 627
Schwarzschild, M. 1954, AJ, 59, 273
Smith, S. 1936, ApJ, 83, 29
Thuan, T. X., & Gunn, J. E. 1976, PASP, 88, 543
Ulmer, M. P., Kowalski, M. P., & Cruddace, R. G. 1986, ApJ, 303, 162
Walker, T. P., Steigman, G., Kang, H., Schramm, D. M., & Olive, K. A. 1991, ApJ, 376, 51
West, M. J., & Richstone, D. O. 1988, ApJ, 335, 532
White, S. D. M., Navarro, J. F., Evrard, A. E., & Frenk, C. S. 1993, Nature, 366, 429
Yee, H. K. C., Ellingson, E., Abraham, R. G., Gravel, P., Carlberg, R. G., Smecker-Hane, T. A., Schade, D., & Rigler, M. 1996a, ApJS, 102, 289
Yee, H. K. C., Ellingson, E., & Carlberg, R. G. 1996b, ApJS, 102, 269 (YEC)
Yee, H. K. C., Sawicki, M. J., Ellingson, E., & Carlberg, R. G. 1996c, in ASP Conf. Proc. 86, Fresh Views on Elliptical Galaxies, ed. A. Buzzoni et al. (San Francisco: ASP), in press
Zwicky, F. 1933, Helv. Phys. Acta, 6, 110
———. 1937, ApJ, 86, 217